Modelling hydrogen injection for internal combustion engines using WENO schemes in the OpenFOAM framework

G. Caramia, P. De Palma

Department of Mechanics, Mathematics and Management

Polytechnic University of Bari, Via Re David 200, 70125 Bari, Italy

Politecnico di Bari

Outlook

- Introduction
- Numerical method
- Simulation set-up
- Grid refinement study
- Results
- Conclusions
- Future work

Introduction

- Hydrogen can be used in internal combustion engines to zero the carbon-based tailpipe exhaust emissions
- In-cylinder direct injection preferable to **avoid** preignition and backfire as well as to **obtain** high volumetric efficiency
- Hydrogen's low density requires **high injection pressures** for fast hydrogen penetration and sufficient in-cylinder mixing
- **Chocked flow conditions** during the injection which result in the formation of turbulent under-expanded jets
- Understanding of the underexpansion process and turbulent mixing just after the nozzle exit necessary for designing of an efficient hydrogen injection system and strategies

Introduction

- Underexpanded jets of hydrogen in air for different Nozzle Pressure Ratios (NPR=P_0/P_∞) investigated

- Schematic of near-nozzle structure of under-expanded jets (picture is based on the visualization presented by Crist et al. [1])

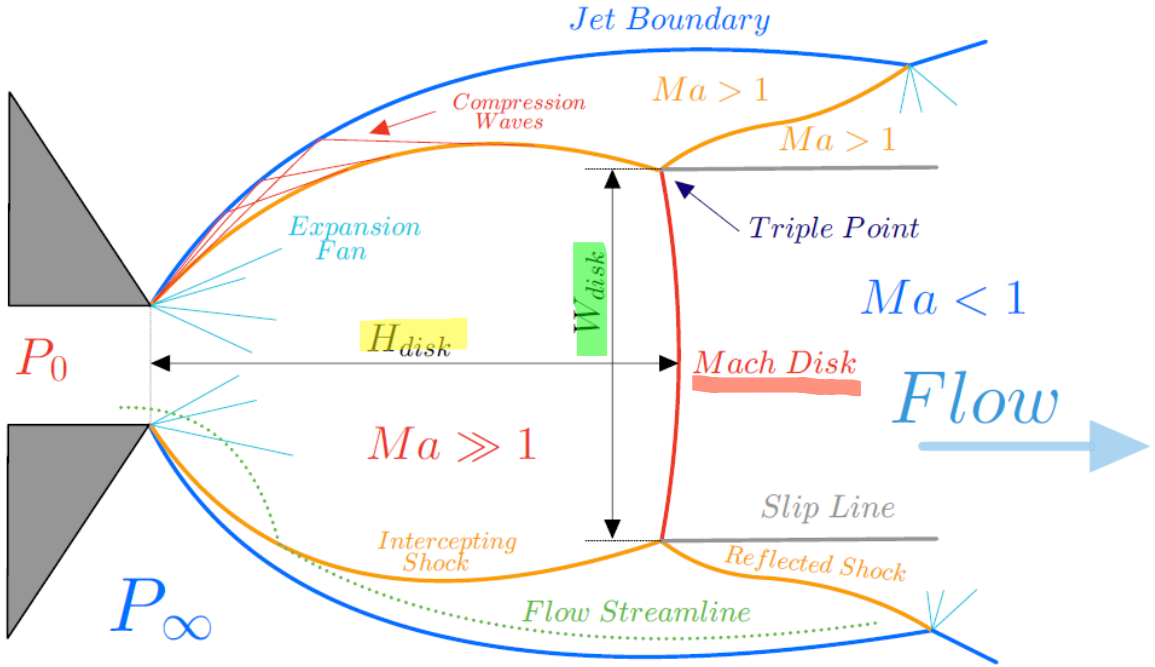

- Very complex flow structures need high accurate scheme with low dissipation and good shock-capturing capabilities. Accurate prediction of H2-air mixing strongly depends on the description of the near-nozzle flow.

Governing equations

The Favre-Reynolds averaged Navier-Stokes equations have been solved with k-ω SST turbulence model

$$\frac{\partial \overline{\rho}}{\partial t} + \frac{\partial \overline{\rho}\tilde{u}_j}{\partial x_j} = 0,$$

$$\frac{\partial \overline{\rho}\tilde{u}_i}{\partial t} + \frac{\partial \overline{\rho}\tilde{u}_j\tilde{u}_i}{\partial x_j} = -\frac{\partial \overline{p}}{\partial x_i} - \frac{\partial}{\partial x_j}\left[(\tilde{\mu}+\mu_t)\left(\frac{\partial \tilde{u}_i}{\partial x_j} + \frac{\partial \tilde{u}_j}{\partial x_i} - \frac{2}{3}\delta_{ij}\frac{\partial \tilde{u}_k}{\partial x_k}\right) - \frac{2}{3}\overline{\rho}\tilde{k}\delta_{ij}\right],$$

$$\frac{\partial \overline{\rho}\tilde{H}}{\partial t} + \frac{\partial \overline{\rho}\tilde{u}_j\tilde{H}}{\partial x_j} = \frac{\partial \overline{p}}{\partial t} + \frac{\partial}{\partial x_j}\left[\left(\frac{\tilde{\lambda}}{c_p} + \frac{\mu_t}{Pr_t}\right)\frac{\partial \tilde{h}}{\partial x_j}\right] + \frac{\partial}{\partial x_j}\left[(\tilde{\mu}+\sigma_k\mu_t)\frac{\partial \tilde{k}}{\partial x_j} + \tilde{u}_i\left(\overline{\tau}_{ij} + \overline{\tau}^R_{ij}\right)\right],$$

$$\frac{\partial \overline{\rho}\tilde{Y}_k}{\partial t} + \frac{\partial \overline{\rho}\tilde{u}_j\tilde{Y}_k}{\partial x_j} = \frac{\partial}{\partial x_j}\left[\left(\overline{\rho}\tilde{D}_k + \frac{\tilde{\mu}_t}{Sc_t}\right)\frac{\partial \tilde{Y}_k}{\partial x_j}\right] + \overline{\dot{\omega}}_k,$$

$$\frac{\partial \overline{\rho}\tilde{k}}{\partial t} + \frac{\partial \overline{\rho}\tilde{u}_j\tilde{k}}{\partial x_j} = \mathcal{D}_k + P^+_k - P^-_k,$$

$$\frac{\partial \overline{\rho}\tilde{\omega}}{\partial t} + \frac{\partial \overline{\rho}\tilde{u}_j\tilde{\omega}}{\partial x_j} = \mathcal{D}_\omega + P^+_\omega - P^-_\omega,$$

Numerical method

- Unsteady RANS using OpenFOAM
- Axisymmetric discretization
- Second-order-accurate Crank-Nicolson time integration
- WENO schemes for advection terms (different orders of accuracy investigated)
- Second-order-accurate linear scheme for diffusion terms
- PIMPLE (combination of PISO and SIMPLE) strategy for pressure-velocity coupling
- rhoReactingPimpleFoam OpenFOAM solver (multi-species solver)

Numerical method

The main idea of WENO schemes is to employ a polynomial representation of the solution at each cell and compute the average value as:

$$\overline{\Phi}_i = \frac{1}{|V_i|}\int_{V_i} \Phi(\vec{x})\mathrm{d}x\mathrm{d}y\mathrm{d}z = \frac{1}{|V_i'|}\int_{V_i'} \Phi(\vec{\xi})\mathrm{d}\xi\,\mathrm{d}\eta\mathrm{d}\zeta = \frac{1}{|V_i'|}\int_{V_i'} p(\vec{\xi})\mathrm{d}\xi\,\mathrm{d}\eta\mathrm{d}\zeta$$

Several polynomial based on different stencils are considered at each cell and a weighted convex combination of them is used.

In the present work the WENO implemetation of

Efficient WENO library for OpenFOAM

Jan Wilhelm Gärtner [a,*], Andreas Kronenburg [a], Tobias Martin [b]

[a] *Institute for Combustion Technology, University of Stuttgart, Herdweg 51, 70174 Stuttgart, Germany*
[b] *Department of Civil and Environmental Engineering, Norwegian University of Science and Technology, 7491 Trondheim, Norway*

published in **SoftwareX 12 (2020) 100611**, has been employed.

Simulation set-up

Nozzle geometry (D=1.5 mm, Hamzehloo et al. [4]) and grid

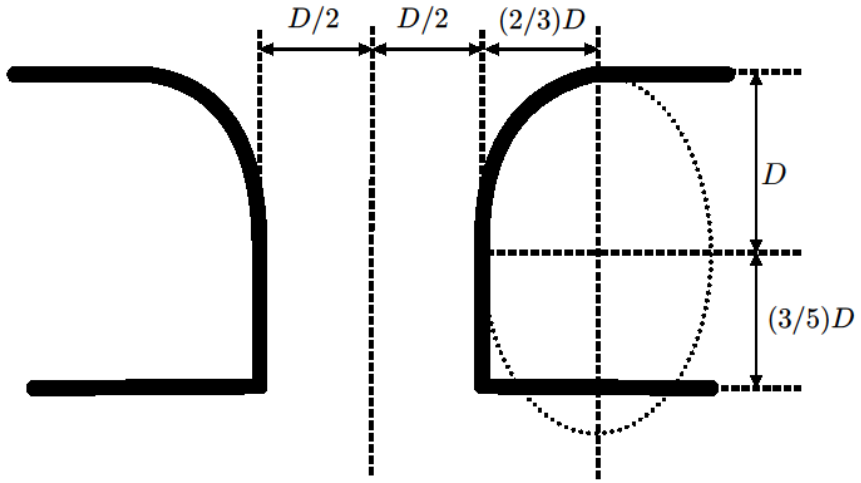

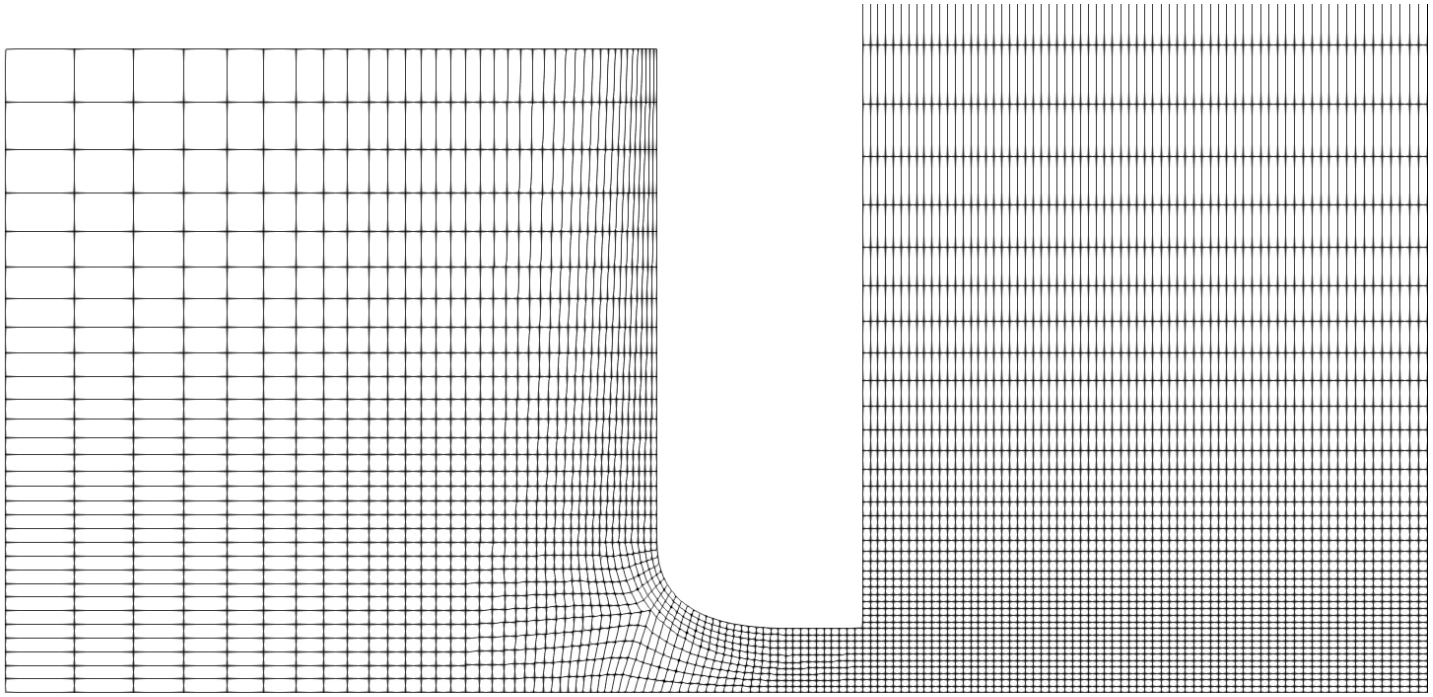

Simulation set-up

"Short" computational domain dimensions (50905 cells)

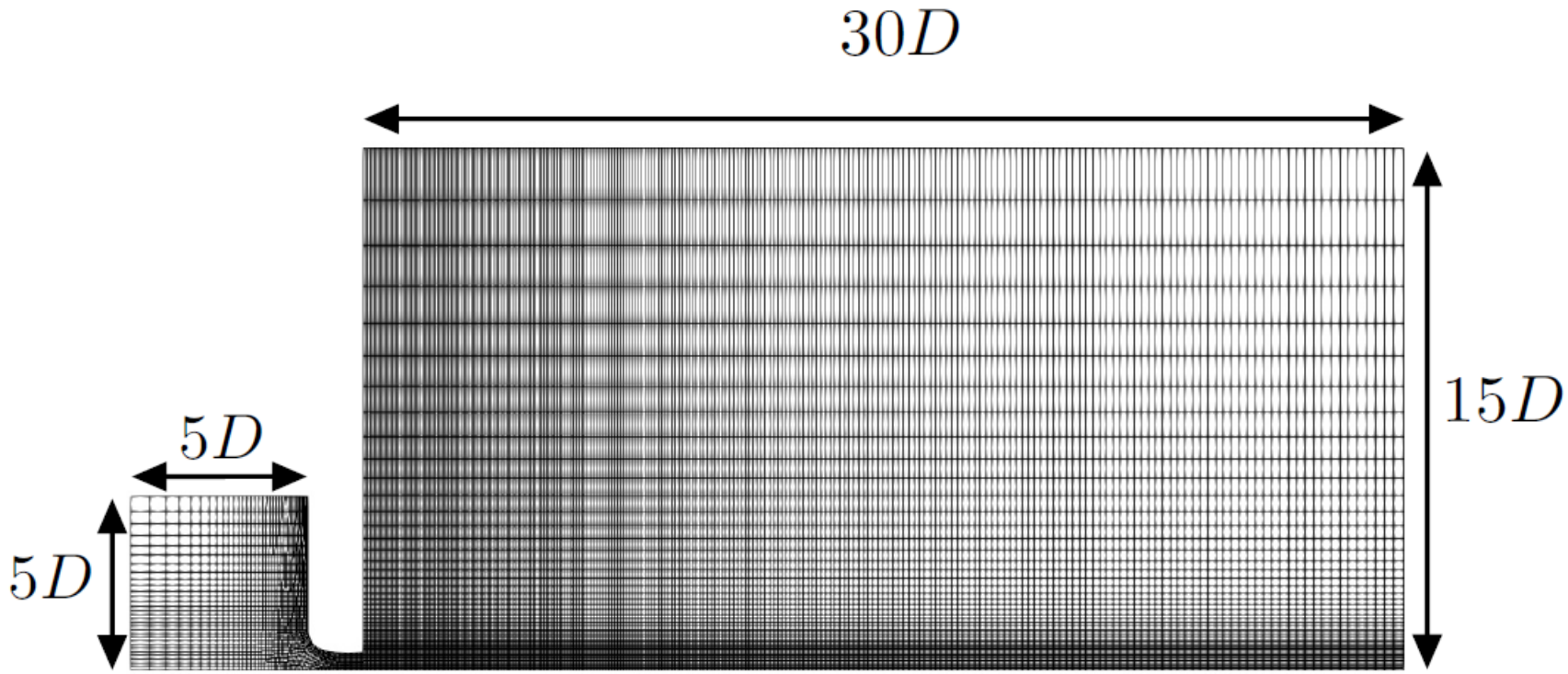

Simulation set-up

"Long" computational domain dimensions (192512 cells)

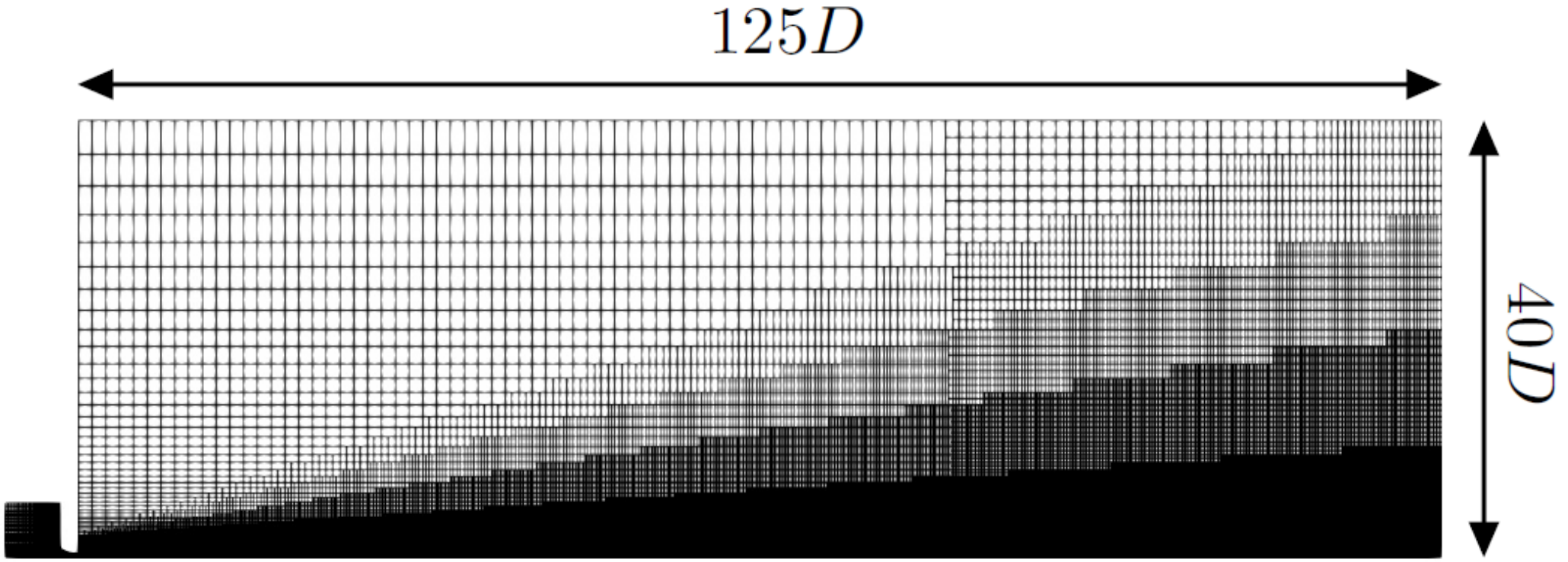

Simulation set-up

Initial and boundary conditions

- **Initialization** (Vuorinen et al. [2])
- **Nozzle wall**: slip, being $Kn \approx 0.1 \div 0.01$ (Gad-el-Hak [3], Hamzehloo et al. [4])
- **Inlet**: total pressure, total temperature, flow angle
- **Outlet**: static pressure (98370 Pa)

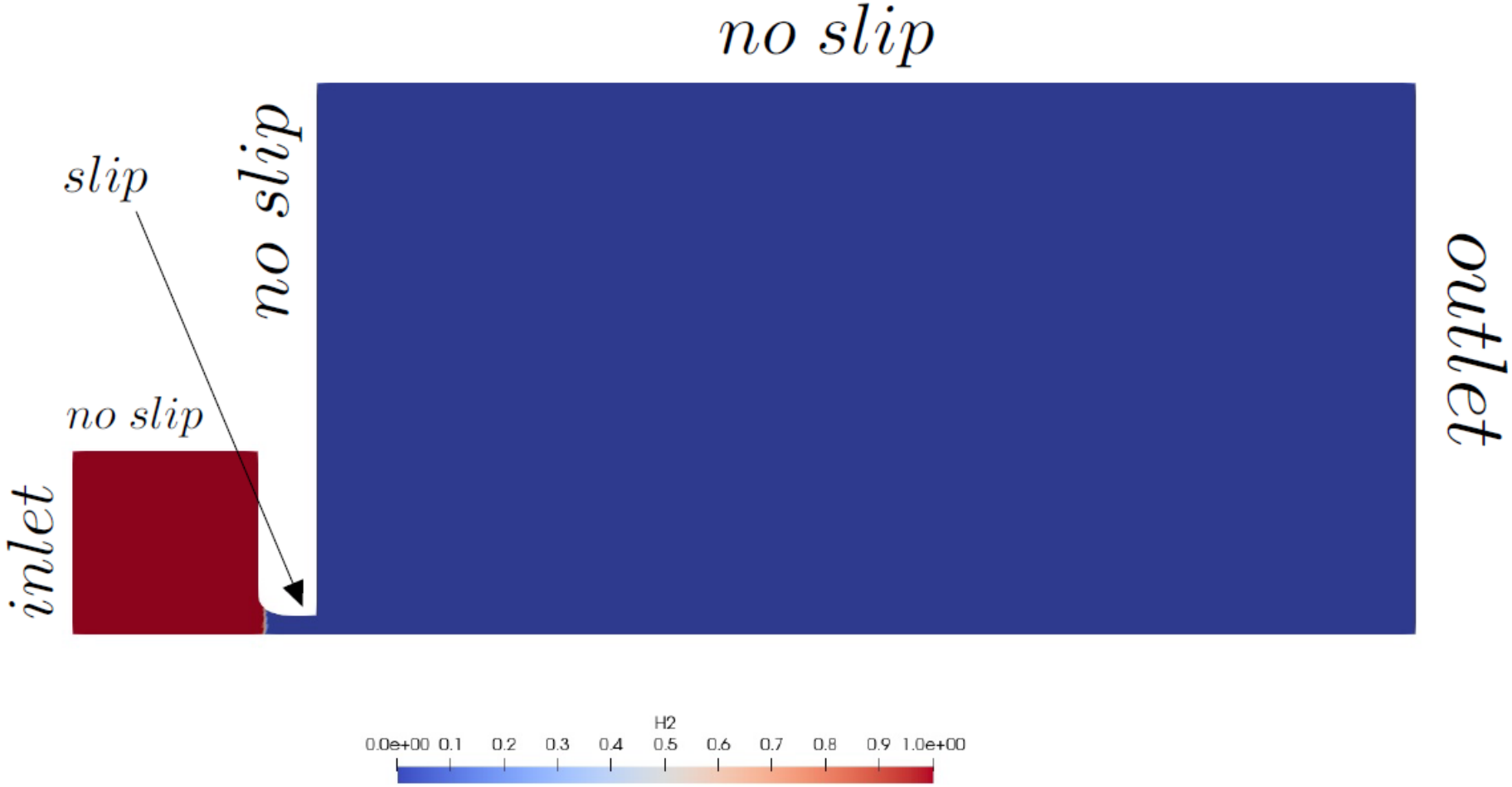

Results

Grid refinement study (NPR=10)

Mach disk **height** [mm] for different grids and schemes: experimental value **3.05** (Ruggles, A. J. & Ekoto I. W. [5])

	*D*10	*D*20	*D*40	*D*80
Linear Upwind	3.62	3.62	3.23	3.07
WENO1	3.65	3.31	3.18	3.27
WENO2	3.74	3.33	3.14	3.17
WENO3	3.79	3.28	**3.09**	3.13

Results

Grid refinement study (NPR=10)

Mach disk **width** [mm] for different grids and schemes: experimental value **1.30** (Ruggles, A. J. & Ekoto I. W. [5])

	*D*10	*D*20	*D*40	*D*80
Linear Upwind	0.36	0.29	1.08	1.25
WENO1	0.39	0.89	1.25	1.36
WENO2	0.40	0.99	1.25	1.18
WENO3	1.09	3.28	**1.27**	1.33

Results

Barrel shock structure (NPR=10, t = 0.2 [ms], WENO 3-0)

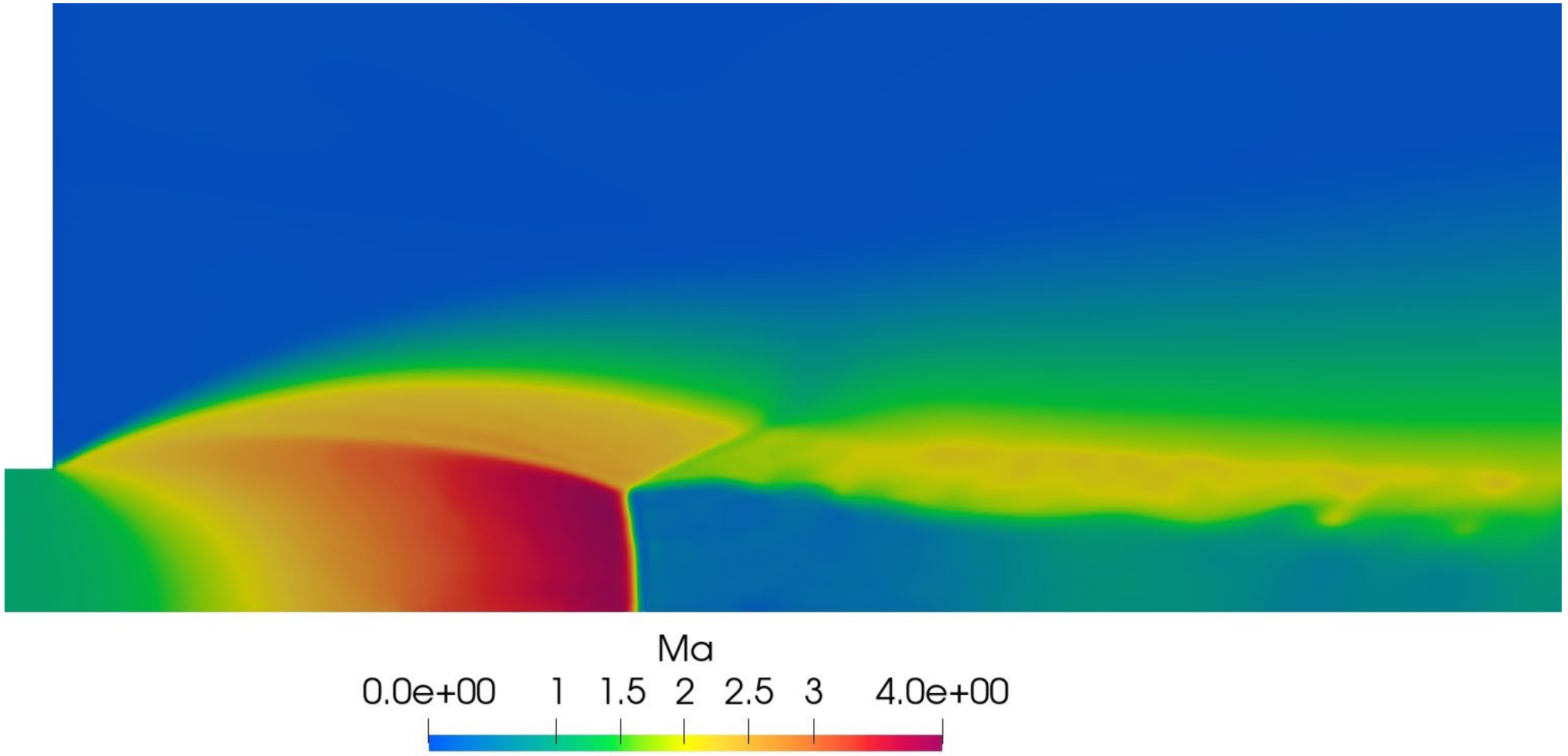

Results

Mach number (t = 0.2 [ms] WENO 3-0)

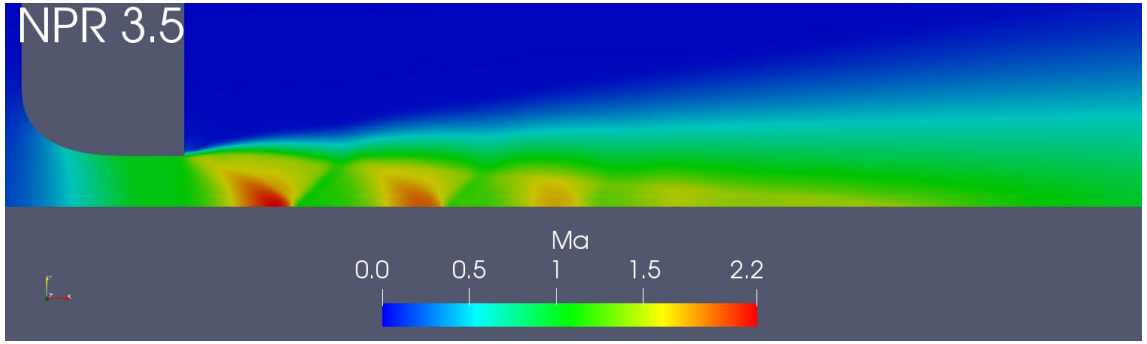

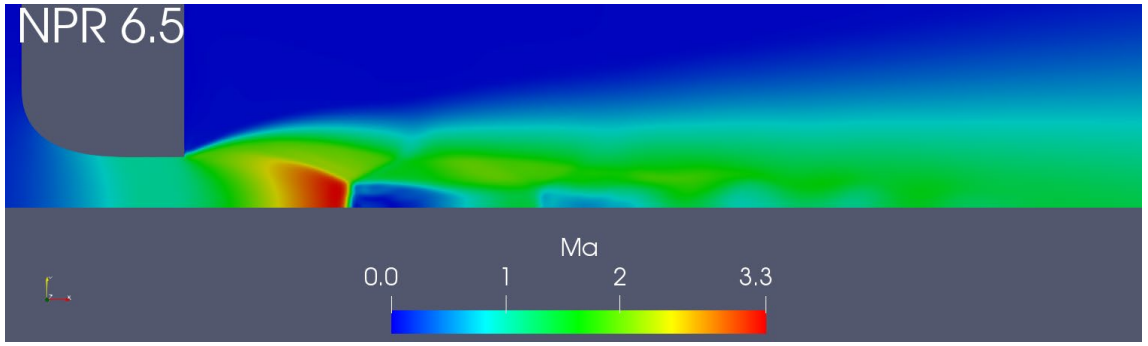

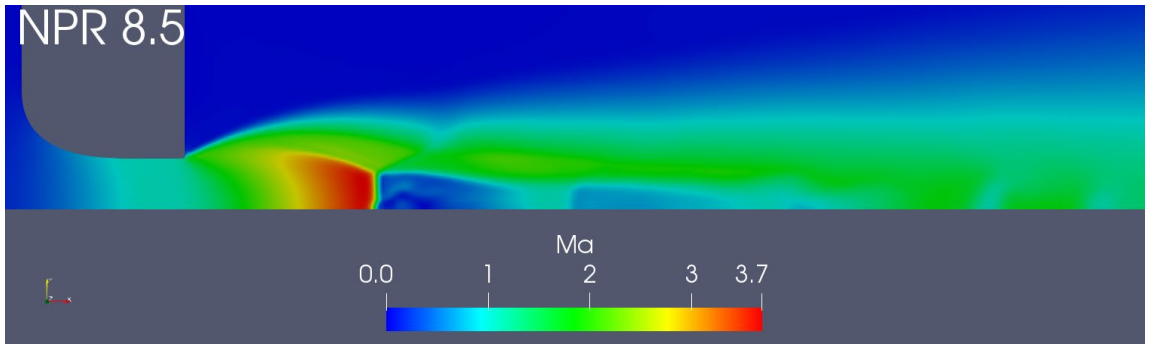

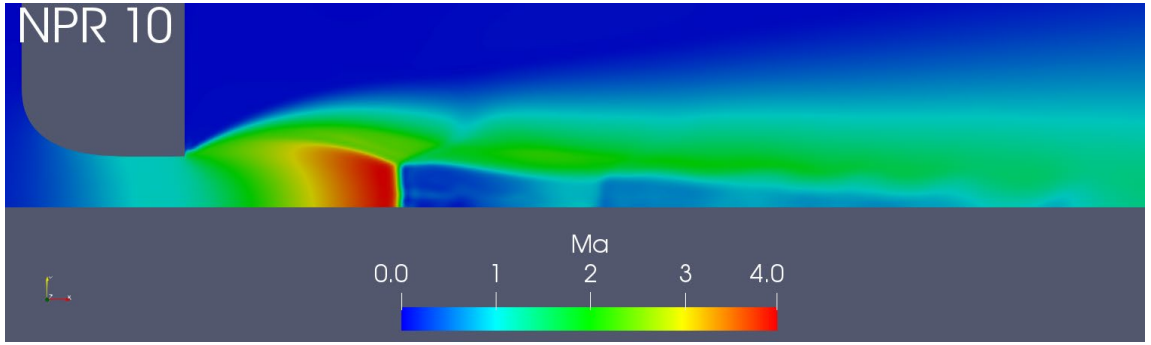

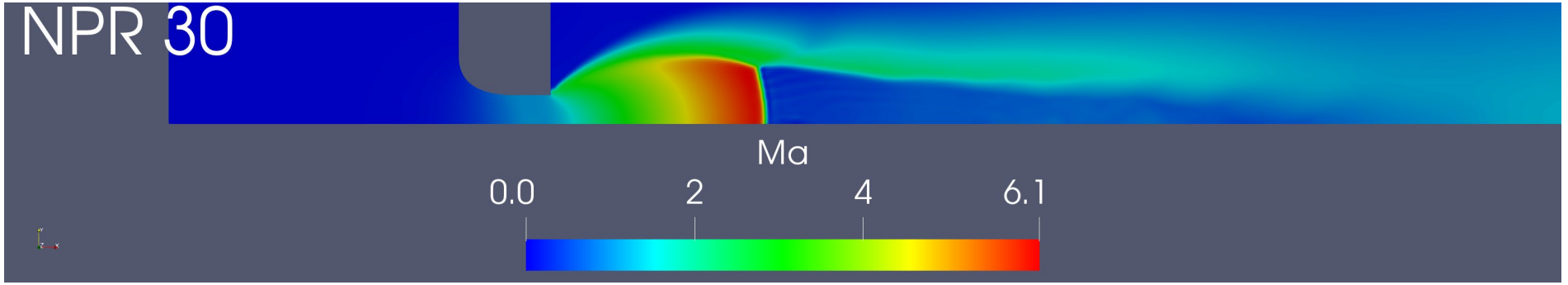

Results

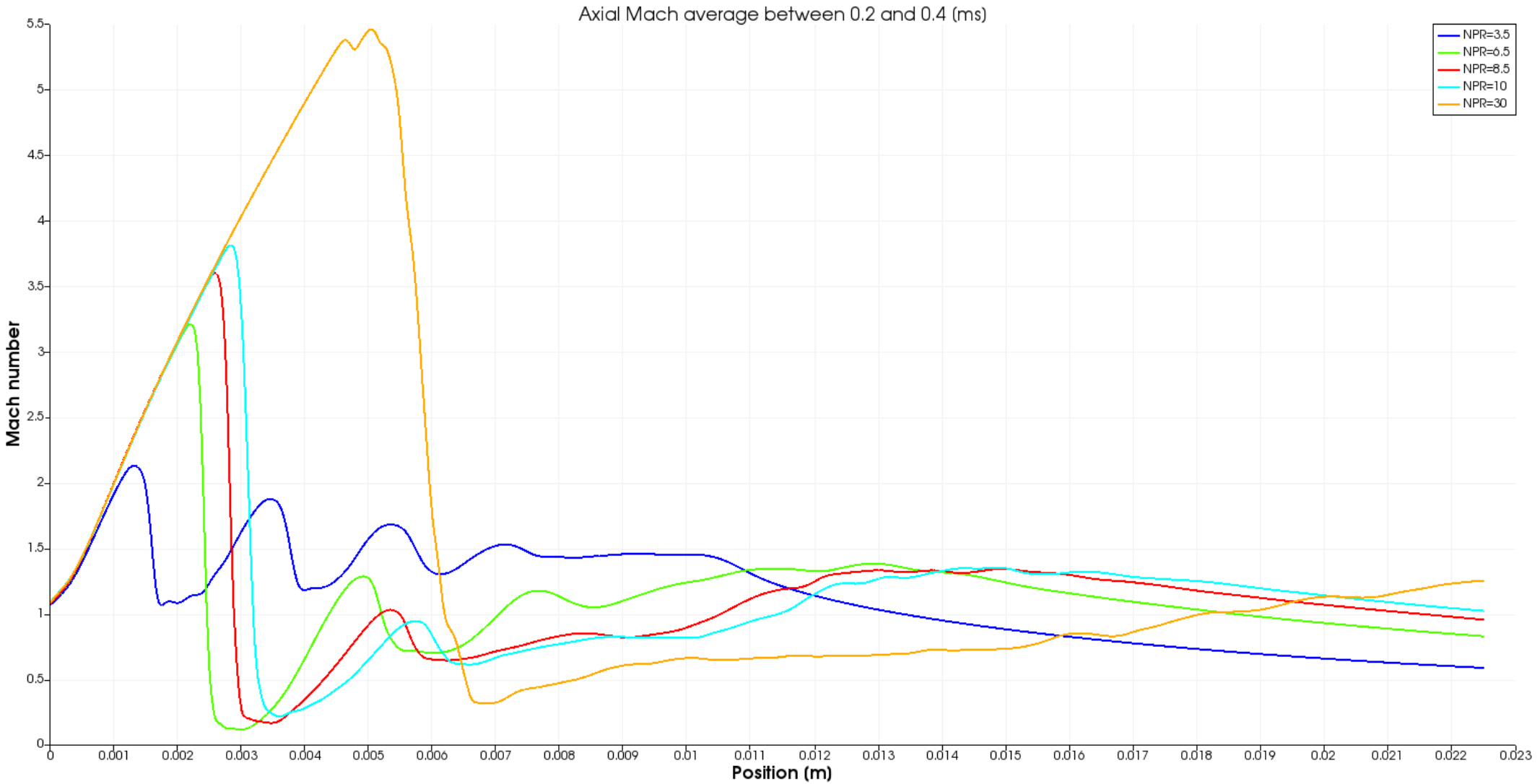
Axial Mach average between 0.2 and 0.4 (ms)
NPR=3.5
NPR=6.5
NPR=8.5
NPR=10
NPR=30
Mach number
Position (m)
0
0.5
1
1.5
2
2.5
3
3.5
4
4.5
5
5.5
0.001
0.002
0.003
0.004
0.005
0.006
0.007
0.008
0.009
0.01
0.011
0.012
0.013
0.014
0.015
0.016
0.017
0.018
0.019
0.02
0.021
0.022
0.023

Results

Kelvin–Helmholtz instabilities only using WENO3 (Temperature [K], NPR = 10)

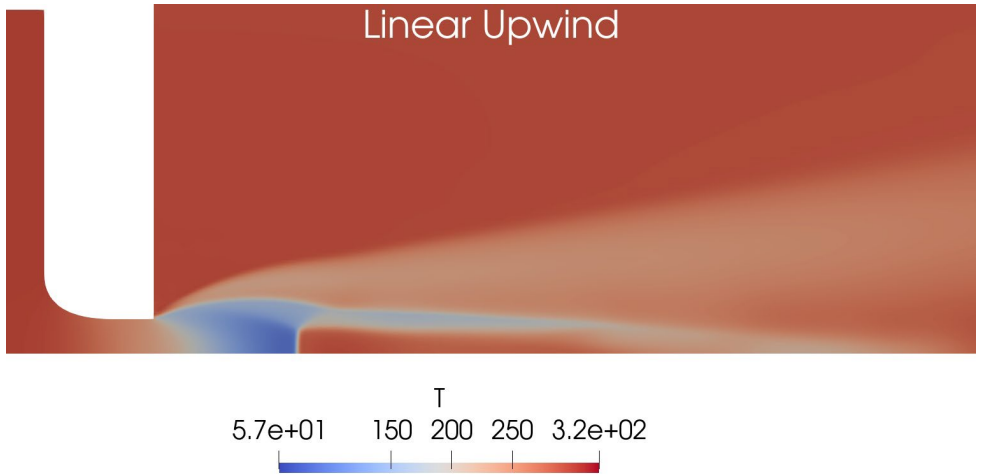

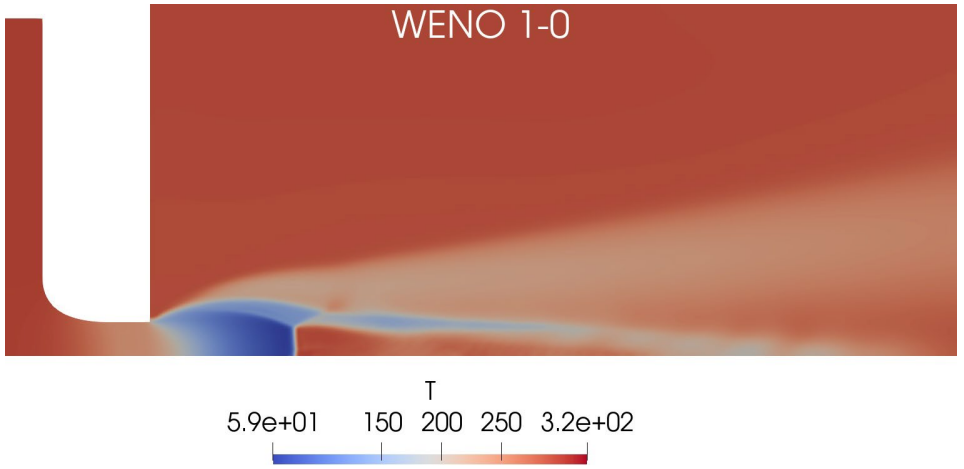

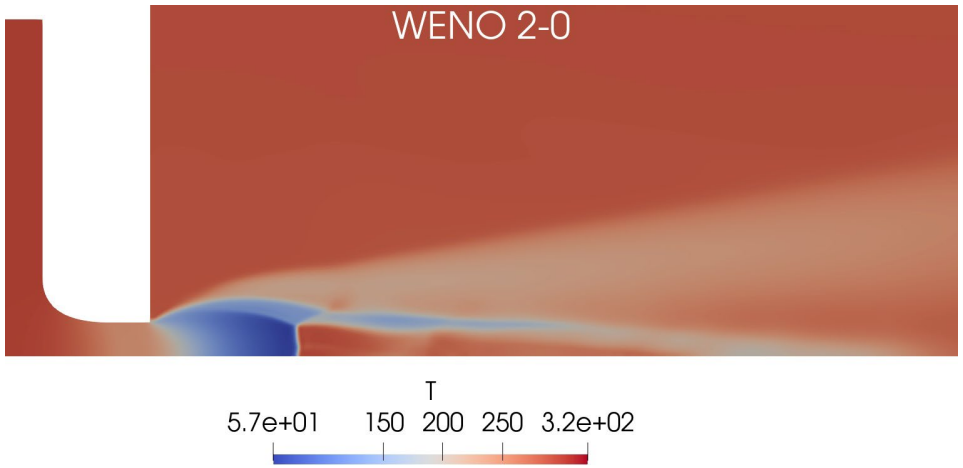

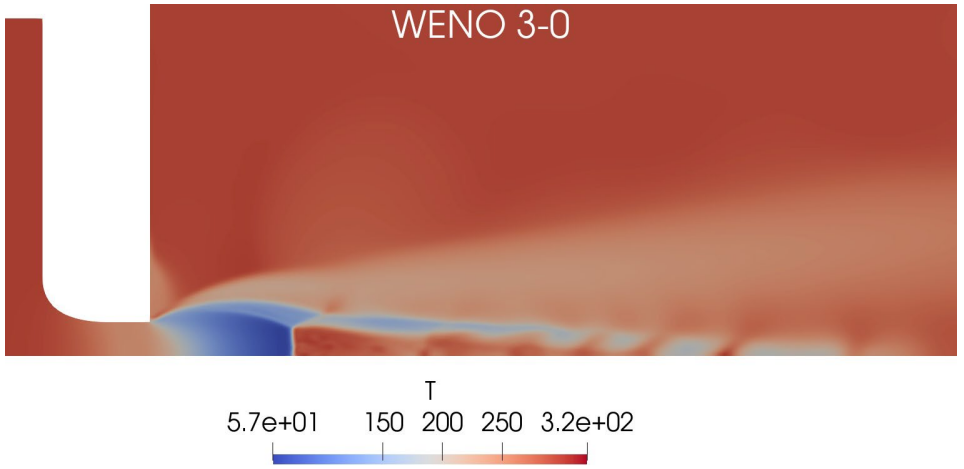

Results

Correlation is a straight line

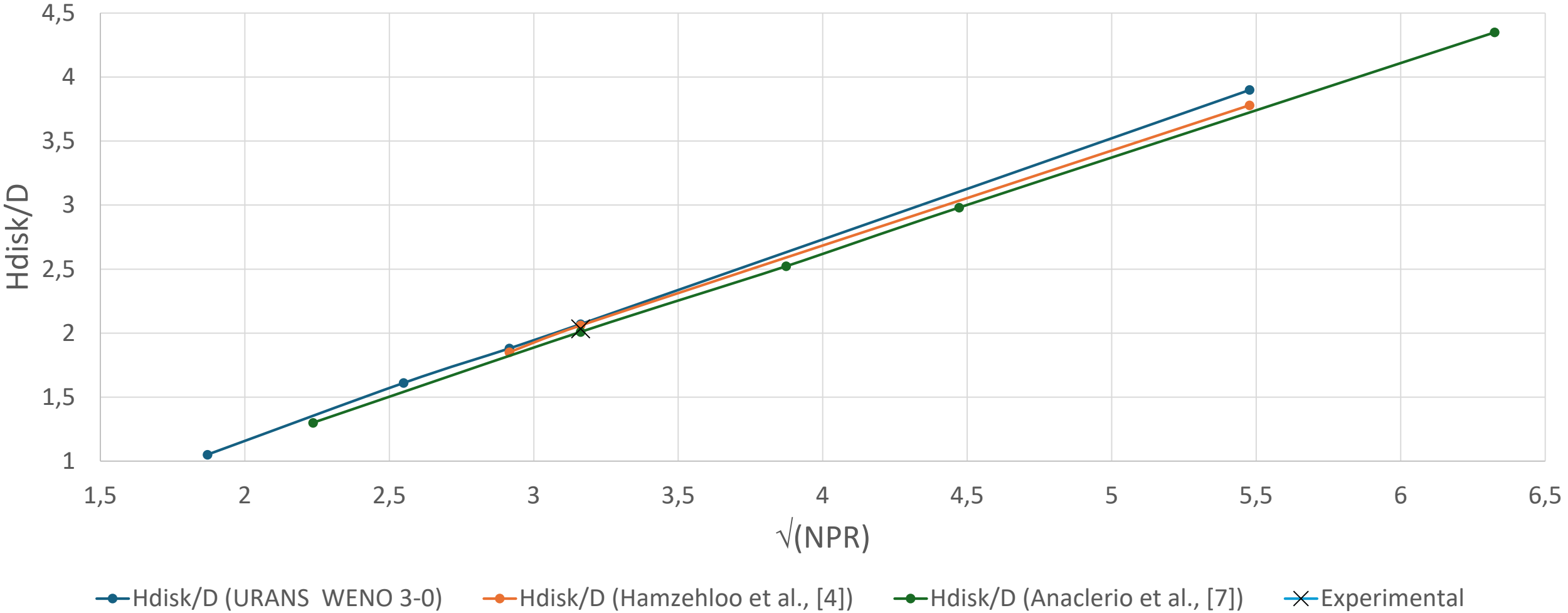

Results

NPR	*Solver*	T_{min} *[K]*	U_{max} *[m/s]*	Ma_{max}
8.5	RANS + WENO 3-0	69	2453	3.7
	LES (Hamzehloo et al. [4])	77	2493	3.72
10	RANS + WENO 3-0	61	2491.6	4
	RANS + WENO 3-1	61.6	2489.8	3.9
	LES (Hamzehloo et al. [4])	71	2531	3.96
30	RANS + WENO 3-0	28	2637.2	6.1
	RANS + WENO 3-1	27.7	2637.2	6.1
	LES (Hamzehloo et al. [4])	41	2695	5.53

Results

H2 mass concentration (Y_{H2}) as a function of distance (Z) from nozzle exit (NPR=10)

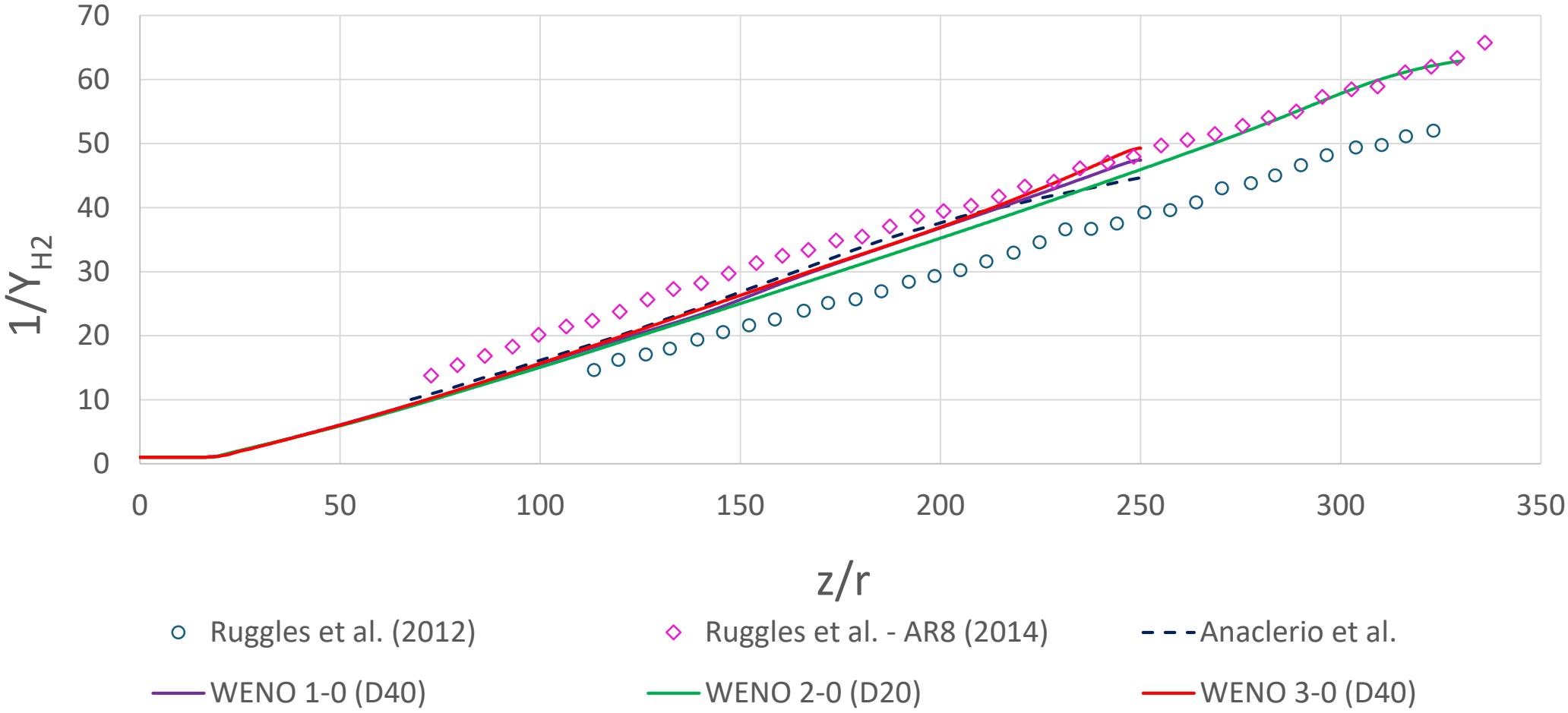

Conclusions

- The near-nozzle under-expanded jet structure and the H2 jet diffusion have been analyzed by an URANS + WENO model
- The method as been validated by a grid refinement study versus experimental and numerical data.
- Linear correlation for Mach disk height at different NPRs has been verified
- The advantage of employing higher spatial order of accuracy is clearly demonstrated by the capturing of coherent structures
- The model tends to overestimate diffusion

Future work

- Improve diffusion model (optimize turbulence model coefficient by a Machine Learning technique)
- Extract POD/DMD modes to construct a reduced order model
- Nozzle geometry optimization by adjoint approach with automatic differentiation
- Extension to 3D-URANS
- Extension to LES

Preliminary 3D Results

~5M cells grid (D40)

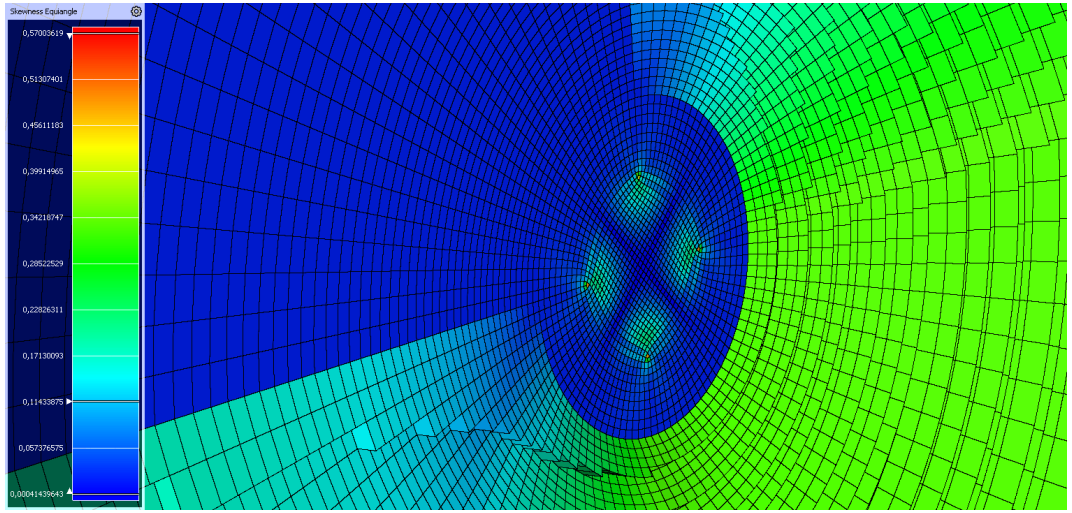

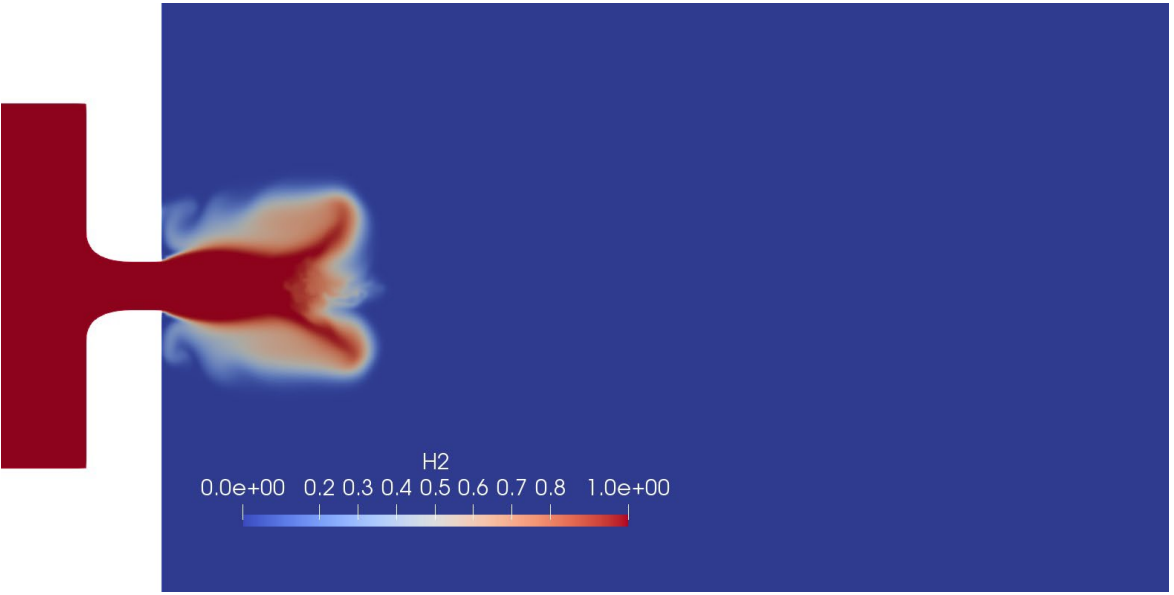

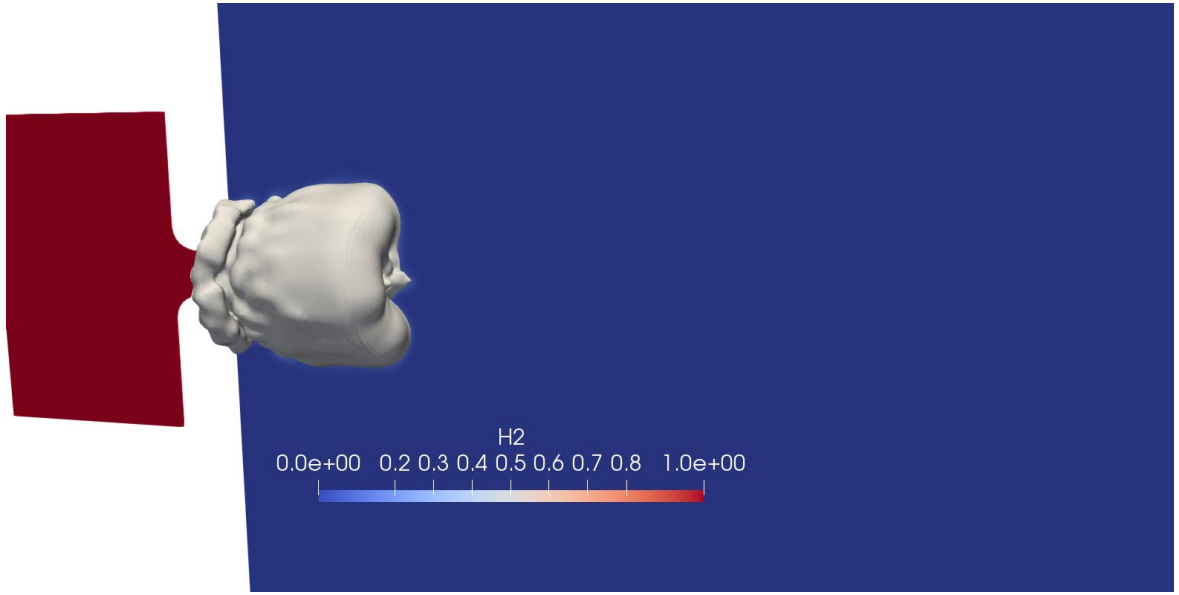

References

[1] Crist, S., Sherman, P. & Glass, D. Study of the highly underexpanded sonic jet. AIAA Journal 1966 4 (1), 68–71.

[2] V. Vuorinen, J. Yu, S. Tirunagari, O. Kaario, M. Larmi, C. Duwig, B. J. Boersma. Large-Eddy Simulation of Highly Underexpanded Transient Gas Jets. Physics of Fluids 1 January 2013; 25 (1): 016101

[3] Gad-el-Hak M. *The fluid mechanics of micro devices - the freeman scholar lecture*. J Fluids Eng 1999:5-33.

[4] Hamzehloo A, Aleiferis PG. *Large eddy simulation of highly turbulent under-expanded hydrogen and methane jets for gaseous-fueled internal combustion engines*. Int. J. Hydrogen Energy, *2014.* 39(36):21275-21296.

[5] Ruggles, A. J. & Ekoto, I. W. 2012 Ignitability and mixing of underexpanded hydrogen jets. International Journal of Hydrogen Energy 37, 17549-17560.

[6] Ruggles, A. J. & Ekoto, I. W. 2014 Experimental investigation of nozzle aspect ratio effects on underexpanded hydrogen jet release characteristics. International Journal of Hydrogen Energy 39, 20331-20338.

[7] Anaclerio G, Capurso T, Torresi M, Camporeale SM. *Numerical characterization of hydrogen under-expanded jets with a focus on Internal Combustion Engines applications*. International Journal of Engine Research. *2023*; 24(8):3342-3358.